UNIVERSITÀ
DEGLI STUDI
DI TRIESTE

Self-Assembly of an Amino Acid Derivative into an Antimicrobial Hydrogel Biomaterial

This is the peer reviewed (post-print) version of the following article:

Original
Self-Assembly of an Amino Acid Derivative into an Antimicrobial Hydrogel Biomaterial / Garcia, A.M., Lavendomme, R., Kralj, S., Kurbasic, M., Bellotto, O., Cringoli, M.C., Semeraro, S., Bandiera, A., De Zorzi, R., Marchesan, S.. - In: CHEMISTRY-A EUROPEAN JOURNAL. - ISSN 0947-6539. - 26:8(2020), pp. 1880-1886. [10.1002/chem.201905681]

Availability:
This version is available at: 11368/2957093 since: 2020-02-06T20:55:51Z
Publisher:

Published
DOI:10.1002/chem.201905681
Terms of use:

Some rights reserved. More details in the PostPrint rights section below.

License:
Attribution-NonCommercial-NoDerivatives 4.0 International

Publisher copyright

-.-

(Article begins on next page)

06 October 2026

arTs Università degli Studi di Trieste
Archivio della ricerca – postprint

Self-Assembly of an Amino Acid Derivative into an Antimicrobial Hydrogel Biomaterial

Ana M. Garcia,[a] Roy Lavendomme,[b] Slavko Kralj,[c] Marina Kurbasic,[a] Ottavia Bellotto,[a] Maria C. Cringoli,[a] Sabrina Semeraro,[a] Antonella Bandiera,[d] Rita De Zorzi,[a] and Silvia Marchesan*[a]

Abstract: *N*-(4-Nitrobenzoyl)-Phe self-assembled into a transparent supramolecular hydrogel, which displayed high fibroblast and keratinocyte cell viability. The compound showed a mild antimicrobial activity against *E. coli* both as a hydrogel and in solution. Single-crystal XRD data revealed packing details, including protonation of the C-terminus due to an apparent pK_a shift, as confirmed by pH titrations. MicroRaman analysis revealed almost identical features between the gel and crystal states, although more disorder in the former. The hydrogel is thermoreversible and disassembles within a range of temperatures that can be fine-tuned by experimental conditions, such as gelator concentration. At the minimum gelling concentration of 0.63 wt%, the hydrogel disassembles in a physiological temperature range of 39–42 °C, thus opening the way to its potential use as a biomaterial.

Introduction

Supramolecular hydrogels formed by protected amino acids or short peptides have become popular biomaterials, by virtue of their simple and low-cost preparation in comparison with longer peptides, as well as their inherent compatibility with biological systems.[1] In the case of single amino acids, examples of self-assembly have been reported thus far, with phenylalanine (Phe) being in a privileged position due to its aromatic and hydrophobic nature.[2] In this case, even the unprotected amino acid self-assembles at very high concentrations in environments as complex as whole cells.[2c] In water, Phe was first reported to form polymorphic systems that featured a mixture of crystals and a gel phase.[3] Simple inclusion of non-gelling additives, such as other amino acids, was a successful strategy to tailor the physical properties of the supramolecular hydrophobic system.[4] In aqueous environments, aromatic interactions and hydrogen bonding play a key role for the self-assembly of low-molecular-weight gelators, and also of their derivatives with polymers.[5]

Hydrogelation of molecules as simple as amino acids can be favored with rigid and aromatic N-capping groups, which reduce the solubility in aqueous media and facilitate hydrophobic interactions that drive the self-assembly. Different examples have been described to date, with fluorenylmethyloxycarbonyl (Fmoc) being the most popular appendage, followed by naphthalene.[2d,6] In particular, the use of a naphthaleneimide N-cap led to fluorescent fibrils, which could be used for imaging purposes.[7] Alternatively, pyrene was successfully applied to obtain a tryptophan-based gel in phosphate buffer at neutral pH for encapsulation of biomolecules.[8] Alkyl-chain N-acylations have also been explored, although prediction of the supramolecular behavior of these derivatives is far from trivial.[9] For instance, in the case of *N*-lauroyl-Phe, self-assembly into the unusual morphology of 2D sheets led to a weak hydrogel;[9] by contrast, *N*-palmitoyl-Phe self-assembled into fibrils that yield a viscous solution.[9]

Small-peptide hydrogels could find useful applications in the area of drug delivery and bioactive biomaterials, for instance in wound healing for burns or diabetic patients.[10] The shorter is the peptide (even a single amino acid), the lower will be the cost of production, and the ease of its scale-up. Additionally, concerns exist over the potential toxicity of polyaromatic cycles, which should be carefully evaluated since cell viability was negatively affected by Fmoc derivatives.[11] Therefore, simpler analogues, which would still allow gelation of small molecules to occur, would be preferable alternatives.[2d]

[a] *Dr. A. M. Garcia, M. Kurbasic, O. Bellotto, M. C. Cringoli, Dr. S. Semeraro, Prof. R. De Zorzi, Prof. S. Marchesan*
Dipartimento di Scienze Chimiche e Farmaceutiche, University of Trieste
Via L. Giorgieri 1, 34127 Trieste (Italy)
E-mail: smarchesan@units.it

[b] *Dr. R. Lavendomme*
Department of Chemistry, University of Cambridge
Lensfield Road, CB2 1EW Cambridge (UK)

[c] *Dr. S. Kralj*
Materials Synthesis Department, Jožef Stefan Institute
Jamova 39, 1000 Ljubljana (Slovenia)

[d] *Dr. A. Bandiera*
Dipartimento di Scienze della Vita, University of Trieste
Via L. Giorgieri 1, 34127 Trieste (Italy)

Results and Discussion

We describe here *N*-(4-nitrobenzoyl)-Phe ability to self-assemble into a nanostructured hydrogel in phosphate buffer saline, PBS, (Figure 1), without the aid of organic solvents. The minimum gelling concentration (MGC) corresponds to 20 mM, that is, 0.63 wt%. TEM imaging (Figure 1 B) reveals low-contrast bundles of fibrils as thin as 5.0 ± 1.1 nm ($n = 100$, see also Figure S7 in the Supporting Information). The hydrogel is thermoreversible with a gel-to-sol transition corresponding to 39–42 °C (Figure 1 C), giving scope to its use for therapeutic applications. If left to cool down to room temperature, the gel reforms within 10 minutes. Increasing the gelator concentration to 30 mM allows the gel-to-sol transition to increase to 54–57 °C, thus confirming that the thermal behavior can be fine-tuned by varying the gelator concentration. Oscillatory rheometry confirms rapid gelation reaching a plateau within an hour (Figure 1 D) corresponding to an elastic or storage modulus *G*′ of 2.0 kPa and a viscous or loss modulus *G*″ of 0.2 kPa. The hydrogel also displays a high resistance[8,12] to applied stress, with a linear viscoelastic regime maintained up to 40 Pa and a gel-to-sol transition occurring at nearly 100 Pa (Figure 1 E). Frequency sweep analysis confirms the gel state, with *G*′ and *G*″ being independent from the applied frequency, and $G' > G''$ (Figure S11 in the Supporting Information). Temperature sweep analysis in the linear viscoelastic regime confirms that the gel-to-sol transition occurs at approximately 40 °C (Figure S12 in the Supporting Information).

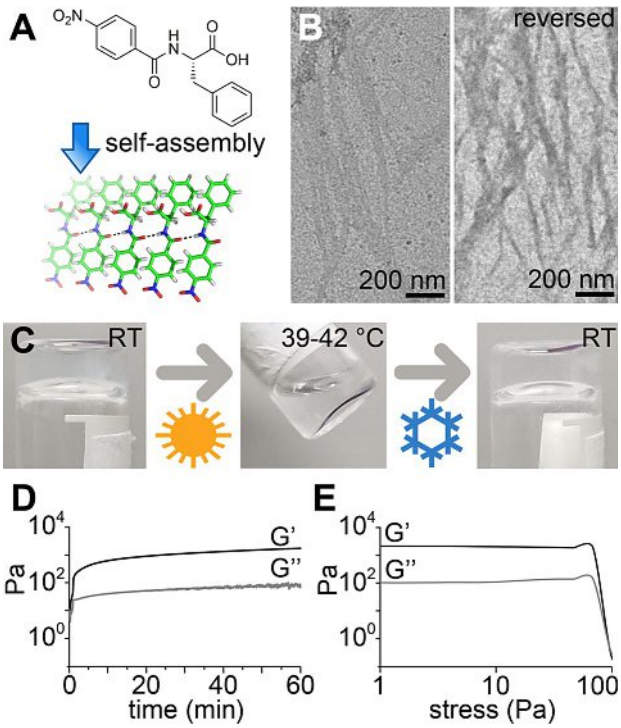

Figure 1. A) *N*-(4-Nitrobenzoyl)-Phe self-assembles into parallel displaced stacks held together by hydrogen bonding ($d = 3.1$ Å) between the amide groups, as revealed by single-crystal XRD data. B) TEM images reveal low-contrast bundles of fibrils as thin as 5 nm, which are present also in the thermoreversed gel (right). C) The 20 mM hydrogel is transparent and thermoreversible within a range compatible with physiological conditions. D,E) Rheology time (D) and stress (E) sweeps show rapid gelation kinetics with plateau reached within 1 hour and high resistance of the gel with failure occurring at nearly 100 Pa.

The secondary structure can be analyzed by several techniques, such as circular dichroism (CD), Fourier-transformed infrared (FT-IR) spectroscopy, and thioflavin T fluorescence (Figure 2 A–C). It should be noted, however, that it is rather controversial to use traditional peptide conformational assignments in cases, like this, in which there is only one amide bond. This has been done purely for the purpose of comparing the spectral data of this work and those reported in the literature and, thus, shedding light on the hydrogen bonding and packing organization. In the far-UV region of circular dichroism (CD) spectra (Figure 2 A), the minima at 220 and 240 nm are dominated by the n–π* transition characteristic of interactions between Phe side chains, thus impeding elucidation of the amide bond environment. The maximum at 280 nm can be attributed to the offset face-to-face stacking of the nitrophenyl rings.[13] Unfortunately, the use of PBS as the solvent for self-assembly impedes CD analysis below 220 nm.

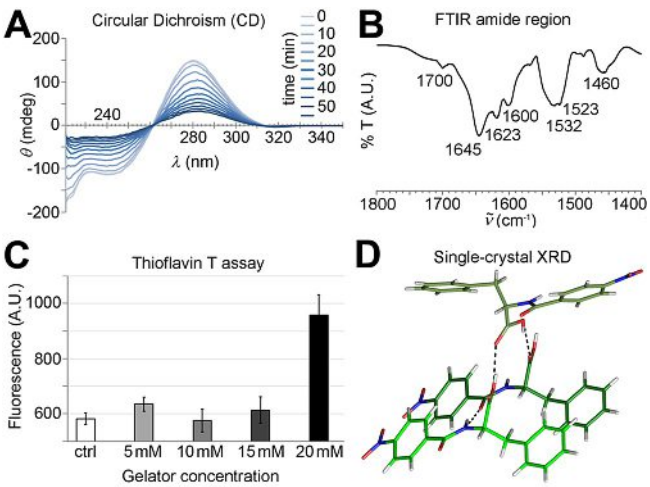

Figure 2. A) CD spectra evolution over 1 h of self-assembly. B) FTIR spectrum (amide I–III region) of the xerogel. C) Thioflavin T fluorescence at various compound concentrations. D) Single-crystal XRD structure showing hydrogen bonds (dashed lines). CCDC 1919220 (see Experimental Section).

The amide I band region of the FTIR spectrum (Figure 2 B) reveals secondary structure signatures, due to the hydrogen-bonding network, in compounds containing even a single amide group that can be used as peptide models.[14] The amide I region is dominated by a peak at 1645 cm^{-1}, which is compatible with disordered structures, and indeed is present also in the FTIR spectrum of the compound in its non-assembled state (see Supporting Information).[15] A minor peak at 1700 cm^{-1} can be assigned to the protonated COOH;[16] this peak is more intense in the powder form, and we inferred this is due to partial deprotonation in the gel state. By contrast, the shoulder at 1623 cm^{-1} arises in the self-assembled state and corresponds to the traditional signature of amyloid fi-

brils.[15a,17] The signal at 1600 cm^{-1} was already reported for Phe-derived supramolecular xerogels, however, it is present also in the FTIR spectrum of *N*-(4-nitrobenzoyl)-Phe in its non-assembled state, and could be due to the aromatic C=C stretching.[15b,18] Finally, the amide III region is dominated by a broad signal centered at 1460 cm^{-1}, which arises with self-assembly. Interpretation of this region is more challenging compared to the amide I, however, the N–H bending signal has been reported to shift down to 1450 cm^{-1} as a result of extended hydrogen bonding and in the presence of inorganic salts.[14a]

A very popular approach to confirm the amyloid-like nature of Phe-derived assemblies is the thioflavin T fluorescence assay (Figure 2C).[2c] The rotation between the two aromatic rings of this dye is limited when it binds laterally to amyloid fibrils, resulting in fluorescence.[19] In silico investigations have shown that the dye binds to aromatic and hydrophobic grooves formed by at least four consecutive β-strands in a linear β-sheet.[20] Interestingly, the dye does not bind to highly charged surfaces, as the binding is not mediated by electrostatic interactions, being instead favored onto neutral species.[21] When performed at different gelator concentrations, the assay results in mild fluorescence only when the MGC is reached (Figure 2C). This data supports the amyloid nature of assemblies, although it also suggests the lack of extended stacks ordered in a similar fashion as peptide β-sheets, in agreement with the considerable amount of disorder noted by FTIR.

Single-crystal XRD analysis (Figure 2D) confirms presence of a hydrogen bond between amides of adjacent molecules, which stack similarly to peptides in β-sheets. Two main hydrophobic interactions are visible in the crystal structure, namely a π–π stacking interaction between the phenyl ring and the nitrophenyl ring of a symmetry-related molecule (located at a distance of 4.7 Å), and a CH–π interaction between two phenyl rings at a distance of 3.1 Å (see Supporting Information, Figure S15). The carboxylic acid terminus appears protonated as it engages in strong hydrogen bonding with two other carboxylic acid moieties with an interatomic oxygen distance as short as 2.7 Å (Figure 2D). Indeed, stacks of carboxylate anions not only would be disfavored due to charge repulsion, but also would not be expected to bind thioflavin T and lead to fluorescence.[21]

In the field of supramolecular systems based on amino acid and peptide derivatives, there is an ongoing debate as to whether the packing arrangement observed in the crystal form is analogous to the one observed in the hydrogel state, since clearly the two solid forms are different, and certainly so both at the macro- and microscopic level. Hierarchical organization of this class of small molecules into supramolecular hydrogels and crystals, as well as the interconversion between the two, indeed is the focus of intense investigations.[22] It is generally accepted that the hydrogel is a kinetic product, whereas the crystal form is the thermodynamic product.[23] To shed light on whether the packing arrangement observed in the crystal form by XRD is relevant to that observed in the hydrogel state, we performed microRaman analysis on both (Figure 3). The very same signals dominated both spectra, with the most dominant

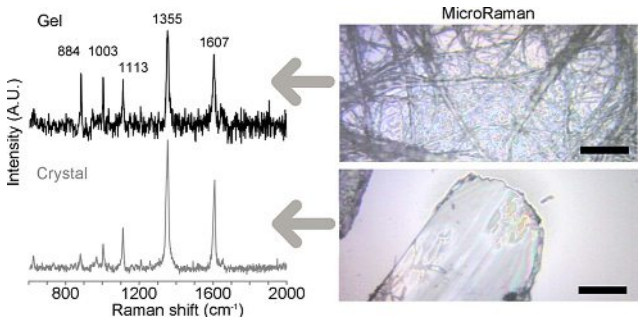

Figure 3. MicroRaman analysis of both the gel and crystal states. Scale bar = 20 microns.

ones being at 1355 cm^{-1} (symmetric stretching of the nitro group),[24] and 1607 cm^{-1} (stretching of C–C bond of the aromatic ring).[25] The signal at 1003 cm^{-1} is also present in both spectra and it is assigned to the breathing mode of the aromatic ring, typically a dominant peak in Raman spectra of Phe derivatives.[25] The signal at 1113 cm^{-1} is not present in the Phe Raman spectra, whereas it has been observed for the 4-nitrobenzoyl moiety.[26] The signal at 884 cm^{-1} is absent in the spectra of 4-nitrobenzoyl chloride[26] and underivatized Phe yet presents as weak signal in those of Phe-containing peptides,[25] and in amino acid N-benzoyl derivatives,[27] thus we infer it can be assigned to the amide N–H bending.[28] Unfortunately, the other amide signals that have been reported to shift based on the hydrogen-bonding pattern are extremely weak in both spectra. In particular, the amide I C=O stretch centered at 1645 cm^{-1} was present in both spectra, as was the amide III band at approximately 1260 cm^{-1}. Overall, the main difference between the Raman spectra of the gel and the crystals lies in the signal intensities, which are significantly higher in the latter. No significant shifts, which are known to occur as a result of different noncovalent interactions or supramolecular environments, are noted. We thus infer that the packing arrangement between the two states is not dramatically different, although it is possible that minor differences related to more disorder in the hydrogel state are not clearly visible, as the signals may simply be too weak to be assigned unambiguously.

The unexpected protonation of the carboxylic acid at neutral pH would appear plausible in the hydrogel, only if accompanied by a pK_a shift of the carboxylic group, due to the self-assembled state interactions. This phenomenon has been previously described for protein and peptides when self-assembled in hydrophobic environments, as well as peptide-derived gelators in their self-assembled state.[29] It can easily be envisaged how otherwise adjacent carboxylate moieties in the supramolecular stacks would result in electrostatic repulsion that would disfavor self-assembly.[29e] The apparent pK_a shift of carboxylic acids was indeed noted with adjacent Phe residues, whereby the highly cooperative competition for hydration between nonpolar and polar species creates repulsive free energy. As a net result, a protonated and neutral state for the carboxylic acid moiety is favored.[30] Indeed, pH titrations at increasing gelator concentrations under MGC confirm a pK_a in-

crease also in the case of *N*-(4-nitrobenzoyl)-Phe from 3.5 at 5 mM to 4.3 at 12.5 mM (see Figure S9 in the Supporting Information); when the solubility limit is surpassed, the heterogeneous system leads to unstable pH readings and considerable noise. Nevertheless, tedious titration experiments with extremely diluted NaOH solutions ultimately showed a pK_a shift up to 6.8 at MGC in PBS (see Figure S10 in the Supporting Information). Although apparent pK_a shifts for COOH groups in N-capped short peptide gelators have been reported,[29a–d] often these do not exceed a pK_a value of 6, thus allowing for the formation of the corresponding hydrogels only at acidic pH.[29a,c]

Overall, the spectroscopic data suggests that the hydrogel shares common features of intermolecular packing with the crystalline state, such as a certain number of parallel stacks with aromatic rings in an offset position. Crystals can be obtained from the hydrogel over a several-week period, confirming the hypothesis that they constitute the thermodynamic and kinetic product, respectively.[23] However, FTIR and fluorescence data suggest that the hydrogel displays a significantly higher level of disordered structures relative to the crystalline state. We infer that the hydrogel contains both protonated and non-protonated carboxyl groups, the latter being bridged by water molecules. It is plausible that, during crystallization, a water molecule gives way to a more stable hydrogen-bonding network due to the intervention of the proton of the COOH group, resulting in the packing shown in Figure 2 D.

In terms of potential applications, *N*-(4-nitrobenzoyl)-Phe was reported to have antimicrobial activity of the same order of magnitude as reference sulfonamides against *S. aureus*, *E. coli*, and *S. enteritidis* when tested in a disk-diffusion assay.[15b] Additionally, intraperitoneal injection in mice revealed an LD_{50} of 6 g kg^{-1} on an average 7-day period.[15b] Encouraged by this data, we reasoned that if the supramolecular hydrogel retained such properties, it would be an attractive candidate for wound healing applications. We were pleased to see high viability for relevant cell types[31] grown on the hydrogel, that is, fibroblasts and keratinocytes (Figure 4 A). In the case of *E. coli*, the hydrogel displays antimicrobial activity, although to a minor extent than the compound in solution at 0.5 mM (Figure 4 B), which we established as the minimum inhibitory concentration (MIC, see Supporting Information),[32] suggesting that fibrillization is not required to exert the bioactivity.

We infer that the antibacterial effect is thus due to the amount of *N*-(4-nitrobenzoyl)-Phe that is released from the gel. This finding is in agreement with observations that Fmoc-Phe also displays antibacterial activity both in the gel and solution phases, thanks to the release of the soluble molecule (from the gel) that exhibits a surfactant-like behavior, as it alters membrane permeabilization and integrity, thus ultimately leading to the death of bacteria.[33]

Conclusions

In summary, this work reports the self-assembly into hydrogels of the amino acid derivative *N*-(4-nitrobenzoyl)-Phe, which has been characterized by several spectroscopic techniques as well as single-crystal XRD and microscopy. A pK_a shift in the self-assembled state is compatible with the presence of protonated carboxylic moieties as revealed by XRD data. Importantly, the hydrogel displays mild antimicrobial activity against *E. coli*, while allowing for high viability of fibroblasts and keratinocytes. Considering that the gel-to-sol transition can occur in the physiologically relevant temperature of 39–42 °C and the antimicrobial activity is maintained by the compound in solution, we think that this material constitutes an interesting starting point for the development of cost-effective, antimicrobial hydrogels for wound healing applications.

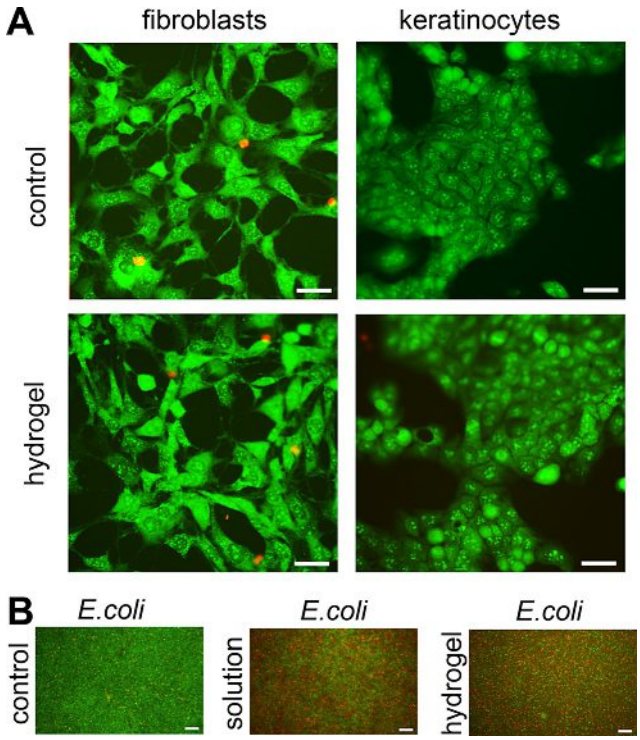

Figure 4. Live(green)/dead(red) fluorescence microscopy on (A) mammalian cells and (B) bacteria. Cells are simply grown on tissue culture plastic surface as a control. Scale bar = 20 μm.

Experimental Section

Materials and methods

All reagents were purchased form Sigma–Aldrich and all solvents were purchased of analytical grade from Merck. High purity Milli-Q-water (MQ water) with a resistivity greater than 18 MΩ cm^{-1} was obtained from an in-line Millipore RiOs/Origin system. ^{1}H NMR spectra were recorded at 400 MHz and ^{13}C NMR spectra were recorded at 100 MHz on a Varian Innova Instrument with chemical shift reported as ppm. ESI-MS spectra were recorded on an Agilent 6120 single quadrupole LC-MS system. Circular dichroism spectra were acquired using a 0.1 mm quartz cell on a Jasco J815 Spectropolarimeter, with 1 s integrations, 1 accumulation and a step size of 1 nm with a bandwidth of 1 nm over a range of wavelengths from 220 to 350 nm at 25 °C (Peltier); samples were freshly prepared directly in the CD cell and the spectra immediately recorded for 1 hour at 25 °C. Oscillatory rheometry was performed on a Mal-

vern Kinexus Ultra Plus Rheometer (Alfatest, Milan, Italy) equipped with a 20 mm stainless steel parallel plate geometry at the temperature of 25 °C in a Peltier system (Alfatest, Milan, Italy). Hydrogels were assembled in situ and measurements were taken immediately with a gap set to 1.00 mm. Kinetics were studied over 60 minutes at a set frequency of 1 Hz and a set stress of 1 Pa. Stress sweeps were measured with a controlled frequency of 1 Hz. FTIR measurements were carried out by using a PerkinElmer 2000 spectrometer. The FTIR spectra were acquired with KBr discs under transmission mode, using the instrument Spectrum software at a resolution of 4 cm^{-1}. The scanned wavenumber range was from 4000 to 400 cm^{-1}. TEM images were acquired on Jeol, JEM 2100, Japan, at 100 kV. TEM grids (copper-grid-supported lacey carbon film) were first exposed to the UV-ozone cleaner (UV-Ozone Procleaner Plus) for 45 mins to make the grid surface more hydrophilic. Then, 24-hour-aged gels were precisely deposited on a TEM grid, dried for 15 min at RT, and contrasted by aqueous tungsten phosphate solution (pH 7.4). Average size and/or cross-section diameter of the nanostructures was determined by taking into account at least 100 individual nanostructures. Raman spectra were acquired on an InVia Renishaw microspectrometer equipped with He–Ne laser (532 nm). Samples were transferred onto a silicon wafer and dried in vacuo prior to analysis. For Raman imaging, the 532 nm laser was focused using the 50× microscope, and the power was set at 0.08 mW. pH titration experiments were performed in MilliQ water unless indicated otherwise; samples were prepared at different concentrations of *N*-(4-nitrobenzoyl)-Phe and the pH was lowered to approximately 2 by addition of HCl; subsequent additions of a solution of NaOH (at the concentrations indicated in the Supporting Information for the different experiments) were performed until no further pH variations were noted and the pH was recorded on a standard pHmeter by using a microelectrode.

Synthesis of *N*-(4-nitrobenzoyl)-Phe

A mixture of L-phenylalanine methyl ester hydrochloride (556 mg, 2.58 mmol), 4-nitrobenzoic acid (360 mg, 2.15 mmol), EDC·HCl (827 mg, 4.31 mmol), HOAt (30 mg, 0.22 mmol) and DIPEA (1.2 mL, 6.9 mmol) in THF (25 mL) was stirred at 50 °C for 5 min to dissolve EDC·HCl then further stirred at room temperature for 80 min. The solvent was then evaporated with a rotary evaporator. The resulting mixture was diluted with 5 mL of CH_2Cl_2 and washed 4 times with 5 mL of aq. HCl (1 M). The CH_2Cl_2 layer was evaporated with a rotary evaporator and the solid was dried under dynamic vacuum affording *N*-(4-nitrobenzoyl)-L-phenylalanine methyl ester as a white solid (679 mg, 2.07 mmol). Yield: 96%. Caution: The peptide coupling reagent 1-hydroxy-7-azabenzotriazole (HOAt) is suspected to be explosive and should be handled with care. Spectral data are in accordance with the literature.[34] ^{1}H NMR (400 MHz, $CDCl_3$, 298 K): $\delta = 8.28$ (d, $J = 8.7$ Hz, 2H, O_2N-ArH), 7.86 (d, $J = 8.8$ Hz, 2H, O_2N-ArH), 7.34–7.24 (m, 3H, -CH_2-Ar, overlapping with $CHCl_3$ signal), 7.11 (dd, $J = 7.6$, 1.7 Hz, 2H, -CH_2-Ar), 6.60 (d, $J = 7.5$ Hz, 1H, NH), 5.09 (dt, $J = 7.6$, 5.6 Hz, 1H, CH-N), 3.80 (s, 3H, O-Me), 3.33 (dd, $J = 13.9$, 5.8, 1H, -CH_2-Ar), 3.24 ppm (dd, $J = 13.9$, 5.8, 1H, -CH_2-Ar).

A suspension of *N*-(4-nitrobenzoyl)-L-phenylalanine methyl ester (531 mg, 1.62 mmol) in MeOH (10 mL) was stirred at 40 °C until complete dissolution. Aq NaOH (1 M, 5 mL, 5 mmol) was then added dropwise and the hot bath was removed. The mixture was further stirred for 30 min while cooling down to RT. Aq HCl (1 M, 10 mL, 10 mmol) was then added dropwise to the stirred mixture. Water (20 mL) were added resulting in the formation of a white gel. Et_2O (20 mL) was added to dissolve the gel. The Et_2O layer was evaporated with a rotary evaporator and dried under dynamic vacuum affording *N*-(4-nitrobenzoyl)-L-phenylalanine as an off-white solid (498 mg, 1.58 mmol). Yield: 98%. The product was purified by reverse-phase HPLC (Agilent Technologies). The HPLC Agilent 1260 Infinity system was equipped with a preparative gradient pump (1311B), semipreparative C-18 column (Kinetex, 5 μm, 100 Å, 250×10 mm, Phenomenex), autosampler (G1329B), Photodiode Array detector (G1315C). The gradient used consisted of acetonitrile (MeCN)/ water with 0.05% TFA with the following program: $t = 0$–2 min 25% MeCN; $t = 12$ min 80% MeCN; $t = 15$ min 95% MeCN; $t = 16$ min 95% MeCN ($t_R = 11$ min). The compound was then freeze-dried to yield the corresponding peptide as a white fluffy powder. Peptide identity was verified by ESI-MS, ^{1}H and ^{13}C NMR. Spectral data are in accordance with the literature and spectra are reported in the Supporting Information.[35] ^{1}H NMR (400 MHz, $CDCl_3$, 298 K) $\delta = 8.26$ (d, $J = 8.9$ Hz, 2H, Ar), 7.83 (d, $J = 8.9$ Hz, 2H, Ar), 7.44–7.25 (m, 3H, Ar), 7.22–7.13 (m, 2H, Ar), 6.62 (d, $J = 7.5$ Hz, 1H, NH), 5.11 (dd, $J = 13.2$, 5.8 Hz, 1H, αCH), 3.39 (dd, $J = 14.1$, 5.7 Hz, 1H, βCH_2), 3.28 ppm (dd, $J = 14.1$, 5.8 Hz, 1H, βCH_2); ^{13}C NMR (100 MHz, $CDCl_3$, 298 K) $\delta = 174.8$ (CO), 165.4 (CO), 149.9 (C-NO_2), 138.9, 135.1, 129.3, 128.9, 128.2, 127.6, 123.9 (C-Ar), 53.6 (αC), 37.2 ppm (βC). MS (ESI) ($C_{24}H_{27}N_5O_4$): *m/z* 314.98 $[M+H]^+$, 336.96 $[M+Na]^+$, 352.93 $[M+K]^+$, 629.00 $[2M+H]^+$, 651.00 $[2M+Na]^+$, 965.16 $[3M+Na]^+$. Note: For the synthesis, commercial HPLC grade MeOH was used as the solvent. CH_2Cl_2 and THF were distilled prior to use.

Gelation protocol

The hydrogel was prepared in phosphate buffer saline (PBS) obtained by dissolving a tablet (#P4417 from Sigma–Aldrich) according to the manufacturer's instructions. The sample with the hydrogelator at a final concentration of 20 mM was heated until complete dissolution and the gel was formed upon cooling down to RT with a final pH of 6.0 ± 0.2. The PBS solution was filtered (0.2 μm) prior to use. For cell culture assays, the PBS solution was first brought to a pH of 11.8 by addition of NaOH; subsequent dissolution of the gelator lowered the pH to 7.3 ± 0.2.

Cell culture

Gelator solutions were sterile filtered and gels were prepared as indicated above (20 μL/well) and prepared directly in triplicate wells of a "μ-Slide Angiogenesis" uncoated (Ibidi, Germany). After 24 h, gels were pre-treated with 30 μL of media (DMEM + 10% fetal serum albumin, and 2% antimycotic and antibiotic from GIBCO) for 1 h. Next, the medium was removed and HaCaT (keratinocytes) or NIH3T3 (fibroblast) cells were added to the gels (10,000 cells per well, 30 μL media), and cultured at 37 °C, 5% CO_2 for 24 h, by handling the slides according to the manufacturer's instructions. Cell viability was investigated by using acridine orange (5 μL/well of a 20 μM solution in 50 mM PBS) and propidium iodide (5 μL/well of a 30 μM solution in 50 mM PBS). Cells were imaged on an inverted microscope (Nikon Eclipse Ti-U) with green and red filters and a 40× objective (N.A. 0.6).

Antibacterial MIC assay

The peptide was dissolved in sodium phosphate buffer (10 mM pH 7.8) to a final concentration of 2 mM and a final pH of 7.2 ± 0.1. All buffer solutions were filtered (0.2 μm) prior to use. Inocula of *E. coli* ATCC 25 922 were prepared by growing cells overnight in Mueller–Hinton (MH) broth. The suspension was diluted with MH to put growing cells to a log phase (1–2 h) to a final optical density (OD_{600}) readings of 0.5–0.7. The bacteria suspension was diluted to 2×10^5 CFU mL^{-1} with MH broth. The minimum inhibitory concen-

tration (MIC) is the lowest concentration of a peptide that prevents visible growth of bacteria. MIC was determined by a standard microtiter dilution method. Cells were grown overnight at 37 °C, 140 rpm in MH broth and were diluted in the same medium. Serial dilutions of the peptides were added into 96-well microtiter plates in a volume of 90 μL/well (2000, 1000, 500, 250, 125, 62, 31 and 15 μM), followed by the addition of 10 μL of bacteria to give final inocula of 2×10^5 CFU mL^{-1} using the formula CFU mL^{-1} = Absorbance (600 nm) $\times 4.6\cdot10^7/0.31$. The plates were incubated at 37 °C for 24 h and the MICs were determined as the lowest peptide concentration that inhibited growth based on OD_{600} readings. Bacteria in PBS or MH broth served as negative controls.

E. coli live/dead assay

All buffer solutions were filtered (0.2 μm) prior to use. The gelator was dissolved in sodium phosphate buffer (10 mM pH 7.2–7.4) to a final concentration of 0.5 mM and a final pH of 7.2 ± 0.1 for the sample "in solution". Alternatively, the hydrogel was prepared as indicated above for cell assays. Inocula of *E. coli* ATCC 25922 were prepared by growing cells overnight in MH broth. The suspension was diluted with MH to put growing cells to a log phase (1–2 h) to final optical density (OD_{600}) readings of 0.5–0.7. The bacteria suspension was diluted to 1000 CFU mL^{-1} with MH broth. In each well of a μ-Slide Angiogenesis uncoated (Ibidi, Germany), 20 μL of solution/hydrogel of peptide were placed in triplicate and left for 24 h at RT, then in each well 10 μL of bacteria suspension (1000 CFU*mL^{-1}) were added and incubated for 24 h. After 24 h of incubation, staining for live/dead bacteria were added (5 μL/well of acridine orange 20 μM in PBS 50 mM and 5 μL/well of propidium iodide 30 μM in PBS 50 mM). Bacteria were imaged on an inverted microscope (Nikon Eclipse Ti-U) with green and red filters and a 60× objective (N.A. 0.7).

Crystallization

Crystals of *N*-(4-nitrobenzoyl)-Phe were grown under the same experimental conditions in which the gel was formed in a closed vial, but at 5 mM over 4 weeks. A single crystal was collected with a loop, cryoprotected by dipping the crystal in glycerol and stored in liquid nitrogen. The crystal structure was solved at the XRD1 beamline at the Elettra synchrotron (Trieste, Italy) and crystallographic data can be found in the Supporting Information.

CCDC 1919220 contains the supplementary crystallographic data for this paper. These data can be obtained free of charge from The Cambridge Crystallographic Data Centre.

Acknowledgements

The authors would like to acknowledge funding from the Italian Ministry of University and Research (MIUR) through the SIR program ("HOT-SPOT" project, personal research grant n. RBSI14A7PL for S.M.), Ramón Areces Foundation (A.M.G. fellowship). R.L. was awarded a postdoctoral fellowship by the Foundation Wiener–Anspach. We acknowledge the financial support from the Slovenian Research Agency (ARRS) for research core funding No. (P2-0089), and the CENN Nanocenter (Slovenia) for the use of electron microscopy. Single-crystal XRD data were acquired at the XRD1 line at the Elettra Synchrotron (Trieste, Italy). Authors acknowledge Prof. J. R. Nitschke for the use of facilities at the University of Cambridge, and Prof. P. D'Andrea at the University of Trieste for fruitful scientific discussions.

Conflict of interest

The authors declare no conflict of interest.

Keywords: hydrogels · phenylalanine · self-assembly · supramolecular chemistry

[1] a) M. A. Sequeira, M. G. Herrera, V. I. Dodero, *Phys. Chem. Chem. Phys.* **2019**, *21*, 11916–11923; b) M. Amit, S. Yuran, E. Gazit, M. Reches, N. Ashkenasy, *Adv. Mater.* **2018**, *30*, 1707083; c) G. Deidda, S. V. R. Jonnalagadda, J. W. Spies, A. Ranella, E. Mossou, V. T. Forsyth, E. P. Mitchell, M. W. Bowler, P. Tamamis, A. Mitraki, *ACS Biomater. Sci. Eng.* **2017**, *3*, 1404–1416; d) P. D'Andrea, D. Scaini, L. U. Severino, V. Borelli, S. Passamonti, P. Lorenzon, A. Bandiera, *Biomaterials* **2015**, *67*, 240–253.

[2] a) S. Bera, S. Mondal, S. Rencus-Lazar, E. Gazit, *Acc. Chem. Res.* **2018**, *51*, 2187–2197; b) M. Mba, D. Mazzier, S. Silvestrini, C. Toniolo, P. Fatás, A. I. Jiménez, C. Cativiela, A. Moretto, *Chem. Eur. J.* **2013**, *19*, 15841–15846; c) L. Adler-Abramovich, L. Vaks, O. Carny, D. Trudler, A. Magno, A. Caflisch, D. Frenkel, E. Gazit, *Nat. Chem. Biol.* **2012**, *8*, 701; d) B. L. Abraham, W. Liyanage, B. L. Nilsson, *Langmuir* **2019**, *35*, 14939–14948.

[3] W.-P. Hsu, K.-K. Koo, A. S. Myerson, *Chem. Eng. Commun.* **2002**, *189*, 1079–1090.

[4] S. M. Ramalhete, K. P. Nartowski, N. Sarathchandra, J. S. Foster, A. N. Round, J. Angulo, G. O. Lloyd, Y. Z. Khimyak, *Chem. Eur. J.* **2017**, *23*, 8014–8024.

[5] a) R. Otter, N. A. Henke, C. Berac, T. Bauer, M. Barz, S. Seiffert, P. Besenius, *Macromol. Rapid Commun.* **2018**, *39*, 1800459; b) W. E. M. Noteborn, D. N. H. Zwagerman, V. S. Talens, C. Maity, L. van der Mee, J. M. Poolman, S. Mytnyk, J. H. van Esch, A. Kros, R. Eelkema, R. E. Kieltyka, *Adv. Mater.* **2017**, *29*, 1603769.

[6] a) V. Singh, K. Snigdha, C. Singh, N. Sinha, A. K. Thakur, *Soft Matter* **2015**, *11*, 5353–5364; b) J. Shi, Y. Gao, Z. Yang, B. Xu, *Beilstein J. Org. Chem.* **2011**, *7*, 167–172.

[7] S.-M. Hsu, F.-Y. Wu, H. Cheng, Y.-T. Huang, Y.-R. Hsieh, D. T.-H. Tseng, M.-Y. Yeh, S.-C. Hung, H.-C. Lin, *Adv. Healthcare Mater.* **2016**, *5*, 2406–2412.

[8] J. Nanda, A. Biswas, A. Banerjee, *Soft Matter* **2013**, *9*, 4198–4208.

[9] R. Martí-Centelles, B. Escuder, *ChemNanoMat* **2018**, *4*, 796–800.

[10] a) N. C. Carrejo, A. N. Moore, T. L. Lopez Silva, D. G. Leach, I. C. Li, D. R. Walker, J. D. Hartgerink, *ACS Biomater. Sci. Eng.* **2018**, *4*, 1386–1396; b) Y. Loo, Y.-C. Wong, E. Z. Cai, C.-H. Ang, A. Raju, A. Lakshmanan, A. G. Koh, H. J. Zhou, T.-C. Lim, S. M. Moochhala, C. A. E. Hauser, *Biomaterials* **2014**, *35*, 4805–4814.

[11] a) J. P. Wojciechowski, A. D. Martin, A. F. Mason, C. M. Fife, S. M. Sagnella, M. Kavallaris, P. Thordarson, *ChemPlusChem* **2017**, *82*, 383–389; b) W. T. Truong, Y. Su, D. Gloria, F. Braet, P. Thordarson, *Biomater. Sci.* **2015**, *3*, 298–307.

[12] a) D. Berillo, B. Mattiasson, I. Y. Galaev, H. Kirsebom, *J. Colloid Interface Sci.* **2012**, *368*, 226–230; b) A. M. Garcia, M. Kurbasic, S. Kralj, M. Melchionna, S. Marchesan, *Chem. Commun.* **2017**, *53*, 8110–8113.

[13] W. Liyanage, W. W. Brennessel, B. L. Nilsson, *Langmuir* **2015**, *31*, 9933–9942.

[14] a) J. Zhao, J. Wang, *J. Phys. Chem. B* **2016**, *120*, 9590–9598; b) N. S. de Groot, T. Parella, F. X. Aviles, J. Vendrell, S. Ventura, *Biophys. J.* **2007**, *92*, 1732–1741.

[15] a) J. Seo, W. Hoffmann, S. Warnke, X. Huang, S. Gewinner, W. Schöllkopf, M. T. Bowers, G. von Helden, K. Pagel, *Nat. Chem.* **2016**, *8*, 692; b) I. Rosca, A. Celia Benchea, V. Şunel, D. Sutiman, D. D. Ortansa, C. B. Zelinschi, C. Stan, C. Cheptea, *Rev. Chim.* **2016**, *67*, 1062–1067.

[16] J. G. Mesu, T. Visser, F. Soulimani, B. M. Weckhuysen, *Vib. Spectrosc.* **2005**, *39*, 114–125.

[17] J. P. Lomont, K. L. Rich, M. Maj, J. J. Ho, J. S. Ostrander, M. T. Zanni, *J. Phys. Chem. B* **2018**, *122*, 144–153.

[18] Y. Yu, N. Chu, Q. Pan, M. Zhou, S. Qiao, Y. Zhao, C. Wang, X. Li, *Materials* **2019**, *12*, 1890.

[19] N. Amdursky, Y. Erez, D. Huppert, *Acc. Chem. Res.* **2012**, *45*, 1548 – 1557.
[20] M. Biancalana, K. Makabe, A. Koide, S. Koide, *J. Mol. Biol.* **2009**, *385*, 1052 – 1063.
[21] C. Wu, M. T. Bowers, J.-E. Shea, *Biophys. J.* **2011**, *100*, 1316 – 1324.
[22] a) C. Yuan, W. Ji, R. Xing, J. Li, E. Gazit, X. Yan, *Nat. Chem. Rev.* **2019**, *3*, 567 – 588; b) A. D. Martin, J. P. Wojciechowski, M. M. Bhadbhade, P. Thordarson, *Langmuir* **2016**, *32*, 2245 – 2250.
[23] J. Wang, K. Liu, R. Xing, X. Yan, *Chem. Soc. Rev.* **2016**, *45*, 5589 – 5604.
[24] C. Passingham, P. J. Hendra, C. Hodges, H. A. Willis, *Spectrochim. Acta Part A* **1991**, *47*, 1235 – 1245.
[25] D. Iglesias, M. Melle-Franco, M. Kurbasic, M. Melchionna, M. Abrami, M. Grassi, M. Prato, S. Marchesan, *ACS Nano* **2018**, *12*, 5530 – 5538.
[26] SDBSWeb: http://sdbs.db.aist.go.jp (National Institute of Advanced Industrial Science and Technology, accessed on 15/12/2019).
[27] R. H. Angus, P. R. Carey, H. Lee, A. C. Storer, K. I. Varughese, *Can. J. Chem.* **1985**, *63*, 2169 – 2175.
[28] C. Westley, Y. Xu, B. Thilaganathan, A. Carnell, N. Turner, R. Goodacre, *Anal. Chem.* **2017**, *89*, 2472 – 2477.
[29] a) E. R. Cross, D. J. Adams, *Soft Matter* **2019**, *15*, 1522 – 1528; b) M. Tena-Solsona, J. Nanda, S. Díaz-Oltra, A. Chotera, G. Ashkenasy, B. Escuder, *Chem. Eur. J.* **2016**, *22*, 6687 – 6694; c) L. Chen, S. Revel, K. Morris, L. C. Serpell, D. J. Adams, *Langmuir* **2010**, *26*, 13466 – 13471; d) F. Rodríguez-Llansola, B. Escuder, J. F. Miravet, *J. Am. Chem. Soc.* **2009**, *131*, 11478 – 11484; e) C. Tang, A. M. Smith, R. F. Collins, R. V. Ulijn, A. Saiani, *Langmuir* **2009**, *25*, 9447 – 9453.
[30] D. W. Urry, D. C. Gowda, S. Peng, T. M. Parker, N. Jing, R. D. Harris, *Biopolymers* **1994**, *34*, 889 – 896.
[31] E. Y. X. Loh, N. Mohamad, M. B. Fauzi, M. H. Ng, S. F. Ng, M. C. I. Mohd Amin, *Sci. Rep.* **2018**, *8*, 2875.
[32] European Committee for Antimicrobial Susceptibility Testing (EUCAST) of the European Society of Clinical Microbiology and Infectious Diseases (ESCMID), *Clin. Microbiol. Infect.* **2003**, *9*, pp. ix – xv.
[33] A. Y. Gahane, P. Ranjan, V. Singh, R. K. Sharma, N. Sinha, M. Sharma, R. Chaudhry, A. K. Thakur, *Soft Matter* **2018**, *14*, 2234 – 2244.
[34] M. G. Woll, E. B. Hadley, S. Mecozzi, S. H. Gellman, *J. Am. Chem. Soc.* **2006**, *128*, 15932 – 15933.
[35] A. Skogh, S. D. Friis, T. Skrydstrup, A. Sandström, *Org. Lett.* **2017**, *19*, 2873 – 2876.